HTML ABSTRACT + LINKS

The spectra of mixed ^{3}He–^{4}He droplets

S. Fantoni
Scuola Internationale Superior di Studi Avanzati (SISSA) and Instituto Nazionale per la Fisica della Materia (INFM), Democritos Modeling Center for Research in Atomistic Simulation (DEMOCRITOS) National Simulation Center, Via Beirut 2-4, 1-34014 Trieste, Italy

R. Guardiola
Departamento de Física Atómica y Nuclear, Facultad de Física, E-46100 Burjassot, Spain

J. Navarro[a)]
Instituto de Fisica Corpuscular (IFIC), Consejo Superior de Investigaciones Cientificas (CSIC)-Universidad de Valencia, Apartado Postal 22085, E-46071 Valencia, Spain

A. Zuker
Institute de Recherches Subatomiques, Institut National de Physique Nucleaire et de Physique des Particules-Centre National de la Recherche Scientifique (IN2P3-CNRS)/Université Louis Pasteur, F-67037 Strasbourg, France

(Received 4 May 2005; accepted 8 June 2005; published online 5 August 2005)

The diffusion Monte Carlo technique is used to calculate and analyze the excitation spectrum of ^{3}He atoms bound to a cluster of ^{4}He atoms by using a previously determined optimum filling of single-fermion orbits with well-defined orbital angular momentum L, spin S, and parity quantum numbers. The study concentrates on the energies and shapes of the three kinds of states for which the fermionic part of the wave function is a single Slater determinant: maximum L or maximum S states within a given orbit, and fully polarized clusters. The picture that emerges is that of systems with strong shell effects, whose binding and excitation energies are essentially determined by averages over configuration at fixed number of particles and spin, i.e., by the monopole properties of an effective Hamiltonian. © *2005 American Institute of Physics*. [DOI: 10.1063/1.1990112]

I. INTRODUCTION

The study of liquid helium in confined geometries is currently an active area of experimental and theoretical research.[1,2] Helium droplets are weakly bound quantum systems, as a consequence of their small atomic mass and the particular form of the associated van der Waals interaction. For ^{4}He, clusters are bound for any number of atoms, while for ^{3}He it takes about 30–32 atoms[3,4] to form a bound system due to the larger zero-point motion and the Pauli principle. The case of mixed ^{3}He–^{4}He clusters is very interesting, since they are made of particles with different statistics and masses interacting through the same potential. The theoretical calculations predict the existence of instability islands for a sufficiently small number of ^{4}He atoms.[5–8]

Experimentally, small helium clusters are produced by free-jet expansion of the gas. Their mass is then measured by diffraction through a transmission grating, followed by a mass spectrometer detector.[9] Pure ^{4}He clusters, containing up to eight atoms, and mixed clusters, containing one ^{3}He and up to six ^{4}He atoms, have been detected using a grating with a 100-nm period,[10] and even the very weakly bound dimer ^{4}He$_2$ has been unambiguously detected.[11] The experimental setup of Ref. 9 has been improved to detect droplet sizes up to 25–30 amu, and very small mixed systems have been definitely identified.[12]

There have been several theoretical studies of a single ^{3}He atom in a medium-size ^{4}He cluster, either through a density-functional approach[13,14] or microscopic method.[15–17] All ^{4}He$_{N_B}$–^{3}He clusters form bound states for $N_B \geqslant 2$. The excess in kinetic energy pushes the ^{3}He atom to the surface, resulting in a quasi two-dimensional wave function similar to the Andreev state describing one ^{3}He impurity in ^{4}He bulk. Recently, the ordering of the single-particle orbital states has been established.[18] Larger combinations of ^{3}He and ^{4}He atoms have been studied employing a nonlocal finite-range density functional.[14,19,20] Previous variational microscopic studies of these mixed systems have been carried out for the ^{4}He$_2$–^{3}He$_2$ cluster,[21] and for clusters with $N_B \leqslant 8$ and $N_F \leqslant 20$.[5] More recently, the diffusion Monte Carlo (DMC) method has been applied to droplets with $N_F \leqslant 3$ and $N_B \leqslant 17$ in Refs. 6 and 7, and with $N_F \leqslant 20$ and $N_B \leqslant 8$ in Ref. 8. The most important result from microscopic calculations[5,8] is the prediction of instability regions, specially when the number of ^{4}He atoms is small; nevertheless, a core with five or more ^{4}He atoms is able to bind any number N_F of ^{3}He atoms.

Our purpose is to analyze the ground state and the low-lying excited states of the ^{3}He atoms in a mixed helium droplet by using the DMC method and relying on the single-particle orbital orderings obtained previously[18] from the study of a single fermion. The resulting spacings resemble those of the rotational spectrum of a diatomic molecule, where the ^{4}He core plays the role of one atom and the ^{3}He is the other atom. At low energies each level is uniquely classified by its angular momentum, but vibrational-like excita-

[a)]Electronic mail: navarro@ific.uv.es

 © 2005 American Institute of Physics

Downloaded 29 Jan 2010 to 147.156.182.23. Redistribution subject to AIP license or copyright; see http://jcp.aip.org/jcp/copyright.jsp

tions appear at higher energies for heavy enough clusters. The adopted filling order for the large number of ^{3}He atoms is therefore $1s\ 1p\ 1d\ldots$, with some attention being paid to a possible $2s$ intruder. We shall concentrate on clusters with eight and 20 bosons, varying the number of fermions. This moderately large number of bosons ensures the existence of several bound excited levels. All calculations have been made using the Hartree-Fock dispersion-B [HFD-(B)] potential of Aziz *et al.*[22] for the He–He interaction.

The paper is arranged as follows. In Sec. II we give some general details concerning the DMC calculation. Section III collects single-fermion results needed later. Section IV deals with the case of two fermions: this system is simple enough to be analyzed in depth for a large set of quantum numbers, shedding light, in particular, on the single-particle ordering. Section V is devoted to stable mixed clusters, for the specific cases of maximum spin and maximum orbital angular momentum. The case of fully polarized clusters is also considered. In Sec. VI we exhibit the calculated one- and two-body distribution functions, both for normal and fully polarized mixed clusters. Finally, in Sec. VII we summarize our findings and draw some general conclusions.

II. THE DIFFUSION MONTE CARLO METHOD

The DMC[23,24] method is based on an importance sampling wave function, with the double role of controlling the variance of the ground-state energy and incorporating both the required statistics and the desired spin and angular momentum quantum numbers. In this work we use the same form employed previously.[8] The trial wave function is written as the product of four factors,

$$\Psi_T = \Phi_{BB}\Phi_{BF}\Phi_{FF}D_F, \tag{1}$$

corresponding to a Jastrow form for the boson-boson (BB), boson-fermion (BF), and fermion-fermion (FF) parts, and the Slater determinantal part D_F for the fermions. Each Jastrow term is a translationally invariant and symmetric wave function, with the structure

$$\Phi_{MN} = \prod_{i,j} e^{f_{MN}(r_{ij})}, \tag{2}$$

where indices M,N represent bosons (B) or fermions (F), and indices i,j run over the corresponding atoms. The product runs over all different pairs $i<j$ if $M=N$, and no restrictions apply when $M\neq N$. We have used a simple but, nevertheless, physically complete representation

$$f_{MN}(r) = -\frac{1}{2}\left(\frac{b_{MN}}{r}\right)^{\nu_{MN}} - rp_{MN}, \tag{3}$$

depending on three parameters, b, p, and ν, in general, different for each of the three BB, BF, and FF pairs. The short-range coefficients b and ν have been fixed, independently of the number of bosons or fermions, to the values $\nu=5.2$ for any subset MN, $b_{BB}=2.95$ Å, $b_{BF}=2.90$ Å, and $b_{FF}=2.85$ Å. The long-range part rp_{MN} entering Eq. (3) has the role of confining the system and fixing roughly its size. The three parameters p_{MN} are adjusted for each droplet by minimizing its ground-state energy.

The last factor D_F in the trial wave function is the determinantal part, which will be discussed later on for each specific case. The description of the trial wave function is completed by the inclusion of the Feynman-Cohen backflow[25] in the fermionic exponential tail as well as in the radial dependence of the Slater factor. Following Ref. 26, we have replaced each fermion coordinate $\mathbf{r}_i$ by a transformed coordinate

$$\hat{\mathbf{r}}_i = \mathbf{r}_i + \sum_{i\neq j} \eta(r_{ij})(\mathbf{r}_i - \mathbf{r}_j). \tag{4}$$

For the backflow function $\eta(r)$ we choose the medium-range form used in Ref. 27:

$$\eta(r) = \frac{\lambda}{r^3}, \tag{5}$$

keeping the same value for the parameter $\lambda=5$ Å^3.

Using the model described above for the importance sampling guiding function, a real-time DMC evolution has been carried out employing a $\mathcal{O}(\tau^3)$ approximation to the Green function, with time slice $\tau=0.000\,25$ K^{-1}, for a total of 200 blocks of 200 steps each. A block average was used in order to diminish the unavoidable correlations of the DMC method, with the aim of obtaining a reasonable estimate of the variance. An initial population of 1000 walkers lead, on the average, to a total number of 40×10^6 samples.

In spite of this block averaging, the resulting estimate of the variance turned out to be quite optimistic, i.e., much smaller than reasonably expected. As a consequence, we opted for a very costly but safe procedure by carrying out ten independent calculations with the same time slice and the same number of samples, but with randomly selected initial set of walkers. The resulting ten results lead to the *true* variance (or so we hope). The numbers quoted in what follows correspond to this prescription.

Due to the presence of the Slater determinants, the importance sampling function is not definite positive. In our calculations, the random process has been constrained using the so-called fixed-node approximation: any walker attempting to cross a nodal surface is neglected. As it has been shown,[24,23] the use of this approximation leads to an upper bound to the lowest energies.

III. THE ONE-FERMION SYSTEM

The system made of a single ^{3}He atom plus a drop of ^{4}He atom has been recently investigated.[18] For the sake of completeness we summarize in this section the most relevant results for the analysis of systems with more fermions.

As there is only one fermion, the Slater determinant in Eq. (1) becomes a single-particle wave function $\phi_{n\ell m}(\mathbf{r})$ of radial quantum number n and orbital angular momentum ℓ with projection m. Translational invariance is ensured by referring the fermion coordinate to the bosonic center of mass.

Different values of ℓ select a specific angular momentum subspace in which the DMC procedure will drive the wave function so as to minimize the energy. Thus, the radial part of the fermionic wave function can be taken to have the form

Downloaded 29 Jan 2010 to 147.156.182.23. Redistribution subject to AIP license or copyright; see http://jcp.aip.org/jcp/copyright.jsp

TABLE I. Energies of droplets with eight and 20 bosons and one fermion for several values of the angular momentum. The row labeled $N_F=0$ is the system without fermions. The columns labeled ϵ are the separation energies. Values in italics correspond to unbound levels.

	$N_B=8$		$N_B=20$	
Configuration	E (K)	ϵ (K)	E (K)	ϵ (K)
$N_F=0$	−5.14(1)		−33.76(2)	
$1s$	−6.08(1)	−0.94	−35.55(1)	−1.79
$1p$	−5.60(1)	−0.46	−35.15(2)	−1.39
$1d$	*−4.98*(1)	0.16	−34.55(2)	−0.89
$2s$	*−5.10*	0.06	−33.80	−0.04

$$\phi_{1\ell m}(r) = r^{\ell} Y_{\ell m}(\hat{r}), \tag{6}$$

which ensures that there are no radial nodes ($n=1$). These single-particle wave functions do not contain a radial-confining term, because it is already included in the Jastrow part of the importance sampling wave function. Notice that within the DMC procedure it is not possible to obtain excited levels with $n>1$, because this will require the imposition of a strict orthogonality on the physical $n=1$ ground state. Nevertheless, one may use an indirect procedure based on the moment method, which will provide an upper bound to the energy of the radial excited levels.

Table I displays the energy of these one-fermion states as a function of the single-fermion quantum numbers. The quoted energies are slightly different from those of Ref. 18 because of the improved statistics of the present calculation. The ground-state energies of the pure bosonic droplets are also given, so as to define the *separation energies*

$$\epsilon_{n\ell} = E_{n\ell}(N_B, N_F=1) - E(N_B, N_F=0), \tag{7}$$

also quoted in the table. Positive values refer to unbound levels. The energy obtained for the $n=2$, $\ell=0$ excited level is above the dissociation limit for $N_B=8$ or very close to it for $N_B=20$.

The single-particle wave functions of Eq. (6) will be used later to construct model wave functions for systems with two or more fermions. Unfortunately the moment method does not provide a wave function for the radial excitation, and for the calculations of the following sections we will use the simple form

$$\phi_{n=2,\ell=0}(r) = r^2 \tag{8}$$

without any radial node. The lack of nodes may be a deficiency, but the truly important point is that the simple form chosen is linearly independent of the $1s$ state.

IV. THE TWO-FERMION SYSTEM

Adding two ^{3}He atoms to a core of ^{4}He atoms results in a system deeply resembling the helium atom. To a large extent, the bosonic subcluster plays the role of the atomic nucleus, with the two ^{3}He atoms corresponding to the electrons. There are two families of levels, singlet ($S=0$) and triplet ($S=1$). Each of the states is characterized by the configuration, the orbital angular momentum L, the spin S, and the parity P.

TABLE II. Space part of importance sampling singlet (upper part) and triplet (lower part) wave functions for the two-fermion drop.

L^P	Config	Ψ
		Singlet
0^+	$1s^2$	1
0^+	$1p^2$	$\mathbf{r}_1\cdot\mathbf{r}_2$
0^+	$1d^2$	$3(\mathbf{r}_1\cdot\mathbf{r}_2)^2-r_1^2r_2^2$
1^-	$1s1p$	z_1+z_2
1^-	$1p1d$	$z_1r_2^2-3z_2(\mathbf{r}_1\cdot\mathbf{r}_2)z_2r_1^2-3z_1(\mathbf{r}_1\cdot\mathbf{r}_2)$
2^+	$1s1d$	$x_1^2+x_2^2-y_1^2-y_2^2$
2^+	$1p^2$	$x_1x_2-y_1y_2$
2^+	$1d^2$	$(x_1^2-y_1^2)r_2^2+(x_2^2-y_2^2)r_1^2-3(x_1x_2-y_1y_2)(\mathbf{r}_1\cdot\mathbf{r}_2)$
2^-	$1p1d$	$x_1x_2z_2-x_2^2z_1-y_2(y_1z_2-y_2z_1)+x_2x_1z_1-x_1^2z_2-y_1(y_2z_1-y_1z_2)$
3^-	$1p1d$	$x_1(y_2^2-x_2^2)+2x_2y_1y_2+x_2(y_1^2-x_1^2)+2x_1y_1y_2$
4^+	$1d^2$	$(x_1^2-y_1^2)(x_2^2-y_2^2)-4x_1x_2y_1y_2$
0^+	$1s2s$	$r_1^2+r_2^2$
1^-	$1p2s$	$z_1r_2^2+z_2r_1^2$
		Triplet
1^-	$1s1p$	z_1-z_2
1^-	$1p1d$	$z_1r_2^2-3z_2(\mathbf{r}_1\cdot\mathbf{r}_2)-z_2r_1^2+3z_1(\mathbf{r}_1\cdot\mathbf{r}_2)$
1^+	$1p^2$	$x_1z_2-x_2z_1$
1^+	$1d^2$	$(x_1z_2-x_2z_1)(\mathbf{r}_1\cdot\mathbf{r}_2)$
2^+	$1s1d$	$x_1^2-x_2^2-y_1^2+y_2^2$
2^-	$1p1d$	$x_1x_2z_2-x_2^2z_1-y_2(y_1z_2-y_2z_1)-x_2x_1z_1+x_1^2z_2+y_1(y_2z_1-y_1z_2)$
3^+	$1d^2$	$x_1^2(y_2^2-z_2^2)-x_2^2(y_1^2-z_1^2)+y_1^2z_2^2-y_2^2z_1^2$
3^-	$1p1d$	$x_1(y_2^2-x_2^2)+2x_2y_1y_2-x_2(y_1^2-x_1^2)-2x_1y_1y_2$
0^+	$1s2s$	$r_1^2-r_2^2$
1^-	$1p2s$	$z_1r_2^2-z_2r_1^2$

Specific two-fermion states are constructed from the single-particle wave functions (6) by coupling the angular momentum part to the required quantum numbers and by symmetrizing the singlet or antisymmetrizing the triplet radial wave functions. In general, one does not obtain real wave functions, but the remedy is simple. For $M=0$ the result is real. Otherwise, construct two cases for M and $-M$ and either add or subtract them. The wave function thus constructed has no good L_z, but still has a good total orbital angular momentum, and should have no effect on the computed energy.

For the sake of completeness we list in Table II the specific forms thus obtained and used as importance sampling wave functions to drive the DMC stochastic procedure.

The energies obtained from these configurations are displayed in Table III for $N_B=8$ and $N_B=20$. Among these results some lie above the dissociation limit (i.e., the energy of the lowest bound state with the same number of bosons but with a single fermion) and do not correspond strictly to truly bound systems.

It has to be understood that in the results quoted in these two tables, only a single number per row does have a physical sense: the DMC algorithm improves systematically the importance sampling wave function, but because of the use of the fixed-node approximation that improvement only provides a variational upper bound to the energy for each of the

Downloaded 29 Jan 2010 to 147.156.182.23. Redistribution subject to AIP license or copyright; see http://jcp.aip.org/jcp/copyright.jsp

TABLE III. Binding energies, in K, for several states with two fermions and $N_B=8$ (upper table) and $N_B=20$ (lower table) classified by the configuration and angular momentum quantum numbers. Values in boldface correspond to the physically interesting states. The dissociation limit is 6.08 K ($N_B=8$) and 35.55 K ($N_B=20$). The statistical errors of the energies are between 0.01 and 0.02 K. The row labeled Eff, is the prediction of the noninteracting fermion model.

L^PS	$1s^2$	$1s1p$	$1p^2$	$1s1d$	$1p1d$	$1d^2$	$1s2s$	$1p2s$
				$N_B=8$				
0^+0	**7.09**		6.12			4.90	7.07	
1^-0		**6.61**			5.49			6.49
2^+0			**6.15**	5.99		4.88		
2^-0					5.50			
3^-0					5.48			
4^+0						4.85		
0^+1							5.89	
1^+1			**6.19**			5.06		
1^-1		**6.65**			5.65			6.46
2^+1				6.01				
2^-1					5.52			
3^+1						4.89		
3^-1					5.45			
Eff.	7.02	6.54	6.06	5.92	5.44	4.82	6.02	
				$N_B=20$				
0^+0	**37.33**		36.70			35.45	37.33	
1^-0		**37.06**			36.05			36.98
2^+0			**36.74**	36.47		35.54		
2^-0					**36.19**			
3^-0					**36.17**			
4^+0						35.55		
0^+1							**35.68**	
1^+1			**36.74**			35.79		
1^-1		**37.05**			36.27			36.99
2^+1				**36.49**				
2^-1					**36.20**			
3^+1						35.66		
3^-1					**36.15**			
Eff.	37.34	36.94	36.54	36.44	36.04	35.44	35.59	

subspaces with well-defined L, S, and P quantum numbers. To give an example, the state ^1S may have projections on the $1s^2$, $1p^2$, $1d^2$, and other shell-model states, but the mixing will probably not be constructed along the DMC stochastic procedure. Hence, the DMC physically relevant results are those with the larger value of the binding energy for each row. The other configurations with smaller energy are possible interacting configurations, and presumably an optimized linear combination within each row could provide a better binding energy.

Note that among the states involving the $2s$ shell none of them has maximum binding, except $1s2s:{}^3S$ because the configuration is unique. For $N_B=8$ this level is not bound, but it is the last bound one for $N_B=20$. For the other cases the DMC-optimized energies prefer $1s$ over $2s$ orbitals, but $1s2s:{}^3S$ survives because $1s^2:{}^3S$ violates the exclusion principle.

Concentrating on the normal shells $(1s,1p,1d)$, it appears that the binding energies depend basically on the configuration and are almost independent of the coupling within the configuration. Figures 1 and 2 give an idea of this near independence, both for energies and radii. Within a central-field shell-model description, this fact indicates that the *residual interaction* between the two ^{3}He atoms is very small, with energies close to the ones provided by the simple noninteracting picture

$$E(n_1\ell_1,n_2\ell_2)=E_0+\epsilon_{n_1\ell_1}+\epsilon_{n_2\ell_2},$$

where E_0 is the energy of the boson core and $\epsilon_{n\ell}$ are the separation energies defined in Eq. (7) and given in Table I. The corresponding values appear in the last row of Table III, with the exception of the last column, the $1p2s$ configuration, which actually has evolved close to the $1s1p$ configuration.

The rough picture of the two-fermion drops as basically noninteracting fermions bound to a rigid ^{4}He cluster will be refined in Sec. VI by introducing an effective monopole interaction.

V. CLUSTERS WITH MORE THAN TWO FERMIONS: BINDING ENERGIES

In this section we consider selected states with a fixed number of bosons and an increasing number of fermions, up

Downloaded 29 Jan 2010 to 147.156.182.23. Redistribution subject to AIP license or copyright; see http://jcp.aip.org/jcp/copyright.jsp

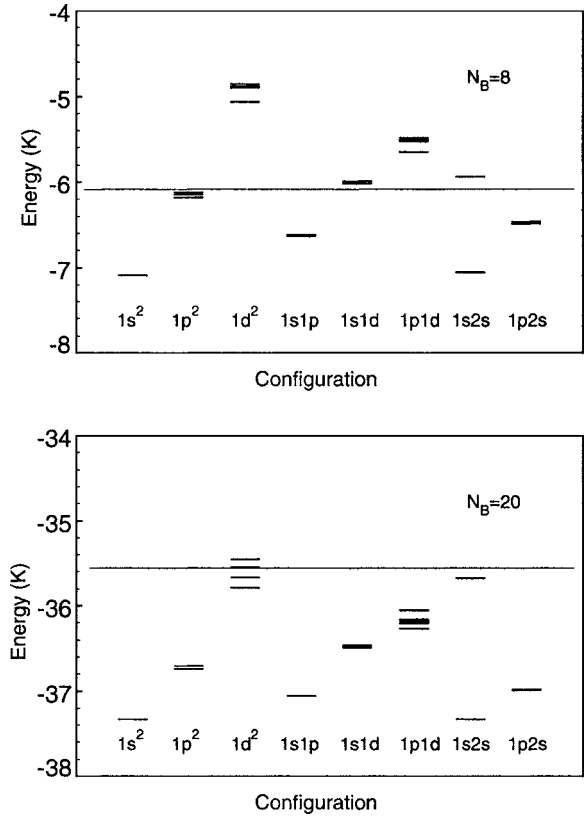

FIG. 1. The two-fermion spectrum for $N_B=8$ and $N_B=20$, classified according to the configuration. Energies are in kelvin. The horizontal line is the dissociation limit. Note that apart from the energy shift, the scales of the two plots are the same.

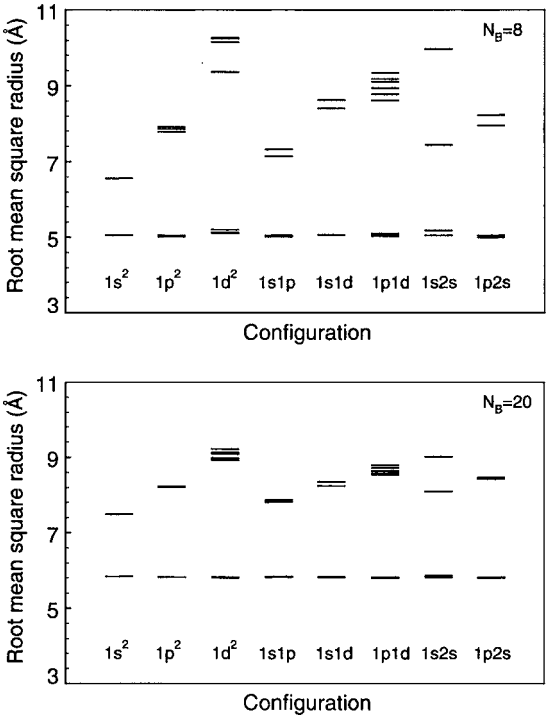

FIG. 2. The root-mean-square radius (in Å) of bosons and fermions for two-fermion systems, referred to the full center-of-mass of the drop, as a function of the configuration. The two plots correspond to $N_B=8$ (upper figure) and $N_B=20$ (lower figure). The lines displaying an almost horizontal line represent the boson radii, and the varying lines represent the fermion radii.

to 18 for normal clusters, i.e., with fermions with spins up and down, and up to nine for fully polarized clusters, with only spin-up fermions.

A. The Slater determinant

The fermionic factor D_F must have good angular momentum and spin quantum numbers, and it must be properly antisymmetrized and translationally invariant. We take it to be a product of two Slater determinants, one for each spin orientation. The obvious way to build them up is with single-particle functions $\phi_{n\ell m}$ generated by a central field which dictates a natural filling order. In general, good total orbital angular momentum L and total spin S demand a linear combination of determinants. If we insist on a single product, the construction is quite cumbersome for shells with high ℓ (see, e.g., Ref. 28), though simple when dealing with s and p shells.

The main problem in establishing a reasonable shell-model description of a system containing ^{3}He atoms, both in pure and in mixed drops, is the lack of phenomenological information about the central field. There are two familiar schemes common to other fermionic systems: the shell ordering $1s,2s,2p,3s,3p,\ldots$ characteristic of atoms and the harmonic oscillator sequence $1s,1p,(2s,1d),(2p,1f),\ldots$ used in light and medium atomic nuclei. The principal quantum number follows different rules in both schemes. For the later the parentheses indicate degenerate orbitals.

In the previous sections we have explained why the $1s,1p,1d,2s,\ldots$ ordering was adopted for the calculations. The information comes from the analysis of a single ^{3}He atom bound to a medium-size bosonic drop, which has been studied by density-functional methods[13,14] and by microscopic methods based either on variational wave functions[15,17] or on DMC techniques.[18] All these studies suggest that the fermion may be viewed as a particle bound to a potential well, centered in the bosonic drop, but which is appreciably different from zero (and attractive) only in a rather wide region near the surface of the drop, and goes to zero near the center of the drop as well as at long distances. This single-particle potential gives a special-level ordering based on the orbital angular momentum, $1s,1p,1d,1f,\ldots$, with almost degenerate single-particle energies. Moreover, the fermion has a very small probability penetrating the boson drop. The same scheme results from the study of one ^{3}He atom in liquid ^{4}He, giving rise to the so-called Andreev states, as well as from the study of many ^{3}He atoms attached to a large core of ^{4}He atoms.[20] Note, however, that *intruder* levels, such as $2s$, may appear for a sufficiently large number of fermions and a sufficiently small number of bosons.

Among the possible wave functions related to a given configuration (the so-called terms in atomic physics), we have chosen the two simplest cases: (a) maximum total spin on which maximum total orbital angular momentum is built and (b) maximum orbital angular momentum on which maximum spin is built. The resulting wave functions are

Downloaded 29 Jan 2010 to 147.156.182.23. Redistribution subject to AIP license or copyright; see http://jcp.aip.org/jcp/copyright.jsp

TABLE IV. Binding energies (in K) of mixed clusters with eight and 20 bosons and up to 18 fermions. Whenever there are two entries for a given cluster, the upper row corresponds to the $S_{\max}$ coupling: particles aligned to maximum S and then to maximum L. The lower row is for the $L_{\max}$ case: maximum L first and then maximum S. In the last column the results obtained in Ref. 8 for $N_B=8$ are also displayed.

N_F	Configuration	L	S	$N_B=8$	$N_B=20$	$N_B=8$ (Ref. 8)
0		0	0	5.14(0)	33.76(1)	5.13(2)
1	$1s^1$	0	1/2	6.08(0)	35.55(1)	6.07(2)
2	$1s^2$	0	0	7.09(0)	37.32(1)	7.05(2)
3	$1p^1$	1	1/2	7.72(0)	38.88(1)	7.69(2)
4	$1p^2$	1	1	8.44(1)	40.47(2)	8.42(2)
		2	0	8.40(1)	40.44(2)	
5	$1p^3$	0	3/2	9.25(1)	42.14(1)	9.23(2)
		2	1/2	9.20(1)	42.08(2)	
6	$1p^4$	1	1	10.09(1)	43.72(3)	10.03(3)
		2	0	10.04(1)	43.71(2)	
7	$1p^5$	1	1/2	11.00(1)	45.40(2)	11.03(3)
8	$1p^6$	0	0	12.00(1)	47.07(2)	12.03(3)
9	$1d^1$	2	1/2	12.49(1)	48.37(2)	12.33(3)
10	$1d^2$	3	1	13.02(1)	49.62(2)	12.74(3)
		4	0	12.97(1)	49.64(4)	
11	$1d^3$	3	3/2	13.65(1)	51.03(4)	13.20(4)
		5	1/2	13.56(1)	51.01(3)	
12	$1d^4$	2	2	14.42(1)	52.46(5)	13.71(5)
		6	0	14.19(1)	52.23(4)	
13	$1d^5$	0	5/2	15.26(2)	53.99(2)	14.20(4)
		6	1/2	14.96(2)	53.71(3)	
14	$1d^6$	2	2	16.01(1)	55.37(4)	14.88(4)
		6	0	15.74(2)	55.19(4)	
15	$1d^7$	3	3/2	16.77(2)	56.83(3)	15.73(5)
		5	1/2	16.64(1)	56.70(5)	
16	$1d^8$	3	1	17.63(2)	58.34(4)	16.55(4)
		4	0	17.62(2)	58.29(4)	
17	$1d^9$	2	1/2	18.64(3)	59.94(3)	17.44(13)
18	$1d^{10}$	0	0	19.74(3)	61.56(5)	18.49(5)

products of two determinants, one for each spin orientation. Other choices demand linear combination of Slater determinants.

As the exponential tail in the trial wave function has the role of roughly confining the system, we can construct the Slater determinants considering only the angular momentum part of the single-particle functions as well as the spin part. As mentioned above, we have used the harmonic polynomials $\phi_{\ell m}(\mathbf{r})=r^{\ell}Y_{\ell m}(\Omega)$ as single-particle functions. The determinants so constructed are translationally invariant wave functions, in the sense that they only depend on the $3N_F-3$ relative coordinates $\mathbf{r}_i-\mathbf{r}_j$. This fact is of crucial importance, particularly when describing systems with a small number of constituents.

The way of constructing the required determinants is very simple. Take for instance the maximum spin case. Once the innermost shells have been filled, the remaining ^{3}He atoms occupy the $\phi_{\ell\ell},\phi_{\ell\ell-1},\ldots$ spin-up states until the angular momentum states are exhausted; then the same procedure is followed to fill out the spin-down states. The spin S of the resulting determinant has the maximum value allowed for the occupancy of the shell, and its orbital angular momentum is $L=|L_z|$. In general, the value of the determinant is a complex number, not very adequate for the DMC algorithm. The solution is as in the two-fermion case: to use the sum or difference (whichever is nonvanishing) of the determinants with $L_z=L$ and $L_z=-L$. The importance sampling wave function has well-defined S, S_Z, and L, but not L_z. Nevertheless, due to the rotational symmetry of the Hamiltonian, this has no influence on the energy values. However, the need for computing determinants with complex matrix elements still remains, with the consequent slowing down of the numerical calculations.

By using this procedure we have calculated states with up to $N_F=18$, corresponding to the complete filling of the three lowest shells. We have also considered states in which all spins are up, i.e., fully polarized fermions, with the maximum number $N_F=9$. The procedure to construct the determinants in this case is an obvious adaptation of the one described above.

In previous works[5,8] we used a conventional Cartesian ordering, in particular, $\{x^2,y^2,z^2,xy,xz,yz\}$, whereby the single-particle orbitals are a mixture of $2s$ and $1d$ wave functions. As a consequence, the differences with the present calculations—associated to changes in the nodal structures—become significant when the d shell starts to be filled.

B. Binding energies of normal clusters

Table IV presents the values of the binding energies corresponding to two situations, $N_B=8$ and $N_B=20$, for values

Downloaded 29 Jan 2010 to 147.156.182.23. Redistribution subject to AIP license or copyright; see http://jcp.aip.org/jcp/copyright.jsp

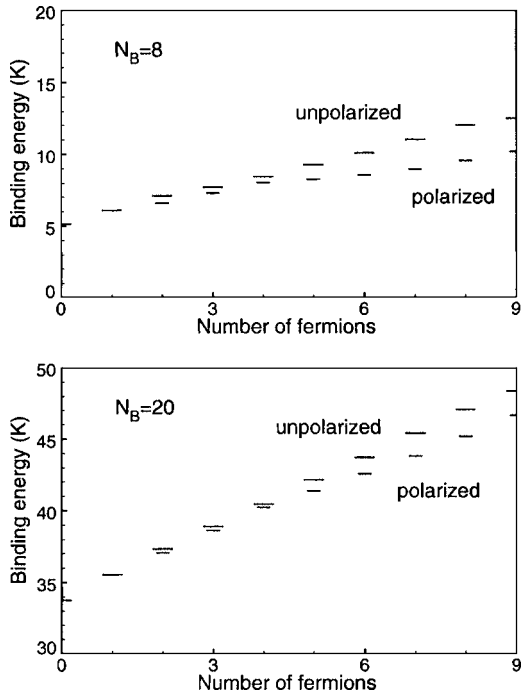

FIG. 3. Binding energies (in K) for $N_B=8$ and $N_B=20$ as a function of the number of fermions N_F. The long horizontal lines correspond to normal clusters, and the short lines to polarized clusters. Note that apart from the energy shift, the scales of the two figures are the same.

of N_F from 0 to 18. All these values have been computed with the level ordering discussed above, and for two possible couplings: $S_{\max}$, where in each shell particles are aligned to maximum spin S, and then to maximum orbital angular momentum L; $L_{\max}$, where particles are first aligned to maximum L, and then maximum S. In Table IV, whenever there are two entries for a given cluster, the upper row corresponds to $S_{\max}$ and the lower one to $L_{\max}$. Maximum spin is quite uniformly favored, but the splitting of the two computed levels is always smaller than 0.3–0.4 K.

The present results for $N_F \leqslant 8$ should coincide, and indeed they do, with previous calculations based on the Cartesian ordering of the single-particle states.[8] Beyond $N_F=8$ the calculations of Ref. 8 used an uncontrolled mixture of $1d$ and $2s$ states, as explained above, thus corresponding to different importance sampling functions. The last column of Table IV displays the results obtained in Ref. 8 for $N_B=8$ clusters. One should keep in mind that both results are based on the DMC method within the fixed-node approximation, so that in both cases the obtained energies are actually upper bounds to the real ones. The present binding energies for $N_F>8$ are slightly higher than the previous results, the gain being of 0.16 K for $N_F=9$ and monotonically increasing up to 1.40 K for $N_F=18$, in the case of $N_B=8$. This apparently modest increase (up to 6%) may be relevant for the boundaries of the stability chart of mixed drops. In any case, it gives support to the level ordering used in the present work, as the associated importance sampling function provides a better variational bound than the previous ones.

The binding energies of Table IV, for normal clusters, have been plotted in Fig. 3 together with those for polarized clusters [to be discussed in Sec. V D (Table V)]. The scale is such that values for the normal clusters are superimposed.

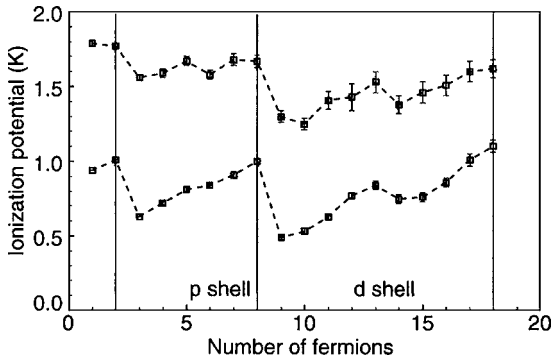

FIG. 4. Separation energies, or ionization potentials, (in K) for normal $S_{\max}$ clusters as a function of the number of fermions N_F. The lower curve correspond to eight bosons, and the upper curve to 20 bosons. The dashed lines are just guides to the eye.

Basically the energies grow linearly with the number of fermions, but finer details emerge when looking at the fermion chemical potential

$$\mu_F(N_F) = E(N_B, N_F - 1) - E(N_B, N_F), \tag{9}$$

which is plotted in Fig. 4 for two values of N_B and $N_F \leqslant 18$. Observe the sudden drop of μ_F after $N_F=2$ and 8, corresponding to the closure of the $1s$ and $1p$ shells. The relative minimum appearing at $N_F=14$ is at first somewhat puzzling. Its origin will become clear in Sec. VI.

C. The stability map revisited

As has been mentioned in the Introduction, one of the most appealing properties of the mixed He clusters is the existence of *instability islands*, namely, regions around selected values of (N_B, N_F) in which the system is not bound. These regions were discovered after many-body computations based on self-adjustable variational functions constructed with Jastrow factors supplemented by $2p-2h$ and $3p-3h$ configuration-interaction correlations.[5] Afterwards, the calculation was refined by means of the DMC method,[8] confirming the previous findings. Given that both calculations really provide only upper bounds to the energy, and having observed the improvement of the present DMC approach, based on a different ansatz for the determinantal part of the importance sampling guiding wave function, we have revised the previous calculation just to check and eventually improve the limits of the instability regions.

Indeed, in Sec. V B we have seen that the present level ordering leads to a noticeable energy gain in the $1d$ shell with respect to previous works. This fact suggests that some of the clusters previously qualified as *metastable*, i.e., systems with negative energy, but less bound than clusters with a smaller number of fermions, could be, in fact, stable. Indeed, a new computation near the beginning of the $1d$ shell indicates two new bound systems, namely, the clusters $(N_B=3, N_F=11)$ and $(N_B=4, N_F=9)$. Special attention has been paid to the cluster $(N_B=1, N_F=18)$, corresponding to full $1s$, $1p$, and $1d$ shells, but our finding is that this cluster is not bound.

Downloaded 29 Jan 2010 to 147.156.182.23. Redistribution subject to AIP license or copyright; see http://jcp.aip.org/jcp/copyright.jsp

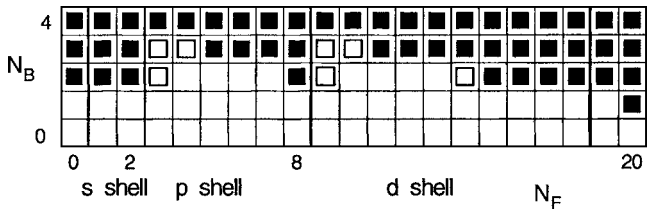

FIG. 5. Stability map of mixed clusters. The solid squares represent truly bound states, and open squares represent metastable states.

The stable clusters are displayed in Fig. 5, which supersedes the results previously obtained in Ref. 8. From the experimental point of view, we suggest the study of the regions $N_B \leqslant 4$ and $N_F \leqslant 5$ to ascertain the stability limits. The measurements will require an improved mass resolution, at least 1 amu for clusters up to 25–30 amu.

D. Polarized mixed clusters

We have also considered fully polarized mixed systems. The values obtained for their binding energies are shown in Table V for $N_B=8$ and 20. In both cases the number of fermions $N_F \leqslant 9$ are limited by the complete filling of the $1s$, $1p$, and $1d$ orbitals. The asterisk in Table V corresponds to situations in which the binding energy of the fully polarized system $E_{\uparrow}(N_B,N_F)$ is smaller than the energy $E(N_B,N_F-1)$ of the normal cluster with one fermion less. In the other cases the results correspond to true bound states.

The energies of polarized clusters are compared with those of normal clusters in Fig. 3. Polarized mixed drops are always less bound than the unpolarized cluster with the same number of fermions. In other words, they are excited states.

The energy differences between normal and polarized clusters take values around 0.25 K ($N_B=8$) and 0.15 K ($N_B=20$) per fermion. It is worth mentioning that theoretical calculations for liquid ^{3}He provide a difference of around 0.10 K per particle at the equilibrium density and −0.10 K at densities close to the solidification one.[29] In other words, the preferred phase would be the polarized one at high densities. This anomalous behavior has been interpreted as a side effect related to improper nodal surfaces for the unpolarized systems. The particle density of the fermionic phase in our case is much smaller than that of the fermionic liquid, and in consequence, we cannot ascertain if our shell-model filling scheme will present such an anomalous crossing at higher densities.

TABLE V. Binding energies (in K) for fully polarized clusters for eight and 20 bosons. The ^{3}He single-particle configuration is indicated in the second column. Results marked with an asterisk correspond to clusters with a binding energy smaller than that of the cluster with one fermion less according to Table IV.

N_F	Configuration	L	S	$N_B=8$	$N_B=20$
0		0	0	5.14(1)	33.76(1)
1	$1s^1$	0	1/2	6.08(1)	35.55(1)
2	$1s^1 1p^1$	1	1	6.65(1)	37.05(2)
3	$1s^1 1p^2$	1	3/2	7.30(1)	38.61(2)
4	$1s^1 1p^3$	0	2	8.06(1)	40.22(1)
5	$1s^1 1p^3 1d^1$	2	5/2	8.26(1)*	41.37(2)
6	$1s^1 1p^3 1d^2$	3	3	8.53(1)*	42.57(2)
7	$1s^1 1p^3 1d^3$	3	7/2	8.96(2)*	43.83(3)*
8	$1s^1 1p^3 1d^4$	2	4	9.53(2)*	45.19(3)*
9	$1s^1 1p^3 1d^5$	0	9/2	10.19(2)*	46.63(2)*

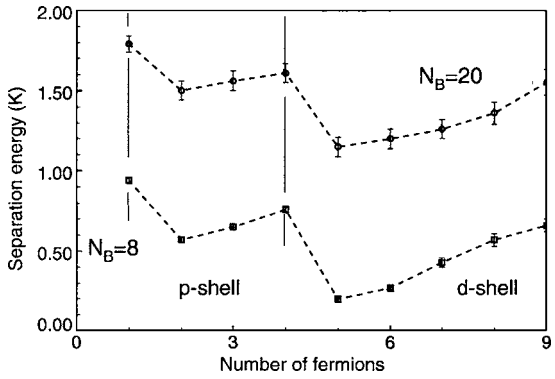

FIG. 6. Separation energies for polarized clusters.

In the same figure one may appreciate a sudden change of the differences $\Delta_E = E_{\text{normal}}(N_F) - E_{\text{pol}}(N_F)$ at $N_F=4$, which has a simple interpretation: it corresponds to the filling of the $1p$ shell for the polarized case and the related jump in the ionization potential after adding a new fermion.

As for the unbound clusters, all of them have very high spin, and their binding energy is larger than the energy of the polarized cluster with one fermion less. Therefore, it is very likely that the set of polarized states corresponds to a stable branch above the dissociation limit, analogous to the so-called displaced terms in atomic physics.

The separation energies for the polarized clusters, displayed in Fig. 6, follow basically the same pattern as the separation energies for the normal clusters. Again they recall the atomic ionization potentials with the sudden drop once a given shell is closed. Note that for polarized fermions the closure of shells occurs at $N_F=1$ ($1s$), $N_F=4$ ($1p$), and $N_F=9$ ($1d$).

VI. EFFECTIVE MONOPOLE INTERACTION ANALYSIS

In this section we shall treat the results of our calculations as data and assume the validity of the shell-model scheme to find an effective one- plus two-body Hamiltonian that could reproduce them. This two-body part will only refer to fermions, as the boson cluster will be assumed as a fixed core that generates the single-particle energies in Table I, leading to a one-body potential.

$$U = \sum_s n_s \varepsilon_s,$$

where n_s is the number of particles in shell s. The sum is extended to the occupied shells.

The two-body part is defined by matrix elements

$$V^{LS}_{rs,tu} = \langle rs:(LS)|V|tu:(LS)\rangle,$$

where $|tu:(LS)\rangle$ is a two-particle state in shells t and s, coupled to orbital angular momentum L and spin S, properly antisymmetrized and normalized.

Downloaded 29 Jan 2010 to 147.156.182.23. Redistribution subject to AIP license or copyright; see http://jcp.aip.org/jcp/copyright.jsp

To simplify matters, the two-body part of the full Hamiltonian will be separated into monopole (m) and multipole (M) contributions $H=H_{mS}+H_M$. The monopole Hamiltonian H_{mS} is defined by the property of giving the *average* energy of configurations at fixed number of particles n_r and spin $\mathbf{S_r}$. The closed shells and the one-particle and one-hole states built on them are configurations with a single state (we call this set $cs\pm1$). Hence, their energies are entirely given by H_{mS}. For the other Slater determinants entering our calculations, H_m gives an average value that will be split by the multipole term H_M. We shall assume (and check) that the influence of H_M is small, and simply neglect it.

The extraction of effective interaction averages goes back in time, and an important earlier reference is the work of French.[30] The form we shall use here came later[31] and was used to describe shell-formation properties in nuclear physics.[32] A forthcoming review article[33] contains comprehensive information on formal properties of H_m and H_M.

The average matrix elements are defined as

$$V_{rs}=\frac{\Sigma_{LS}V^{LS}_{rsrs}(2L+1)(2S+1)(1+(-1)^{L+S}\delta_{rs})}{\Sigma_{LS}(2L+1)(2S+1)(1+(-1)^{L+S}\delta_{rs})},$$

$$V^S_{rs}=\frac{\Sigma_{L}V^{LS}_{rsrs}(2L+1)(1+(-1)^{L+S}\delta_{rs})}{\Sigma_{L}(2L+1)(1+(-1)^{L+S}\delta_{rs})}, \tag{10}$$

where V_{rs} is the full (scalar) average of two-body matrix elements, whereas V^S_{rs} are (vector) averages at fixed S. It is convenient to introduce the following combinations:

$$a_{rs}=\frac{1}{4}(3V^1_{rs}+V^0_{rs}),\quad b_{rs}=V^1_{rs}-V^0_{rs}, \tag{11}$$

$$V_{rs}=a_{rs}-\frac{3}{4}\frac{\delta_{rs}}{D_r-1}b_{rs}, \tag{12}$$

where $D_r=2(2l_r+1)$ is the maximum number of particles in the shell. The standard result is then

$$H_{mS}=U+\sum_{r\leqslant s}\frac{1}{(1+\delta_{rs})}\left[a_{rs}n_r(n_s-\delta_{rs})+b_{rs}\left(\mathbf{S}_r\cdot\mathbf{S}_s-\frac{3n_r}{4}\delta_{rs}\right)\right], \tag{13}$$

where $\mathbf{S}_r$ is the total spin operator corresponding to the particles of shell r, $\mathbf{S}_r=\Sigma_{i\in r}\sigma_i/2$, and the $3n_r/4$ subtraction ensures the two-body nature of H_{ms} by making the spin contribution vanish for *single-particle* states. It has the drawback of producing nonzero values at closed shells and single-hole states. Therefore, it is preferable to rewrite

$$H_{mS}=U+\sum_{r\leqslant s}\frac{1}{(1+\delta_{rs})}\left[V_{rs}n_r(n_s-\delta_{rs})+b_{rs}\left(\mathbf{S}_r\cdot\mathbf{S}_s-\frac{3n_r(D_r-n_r)}{4(D_r-1)}\delta_{rs}\right)\right]. \tag{14}$$

The counter terms in the second line now ensure its vanishing at the closed shell as well as at one-particle and one-hole states. As a consequence, their energies are fully given by the first line in Eq. (14), which we refer to as H_m from now on.

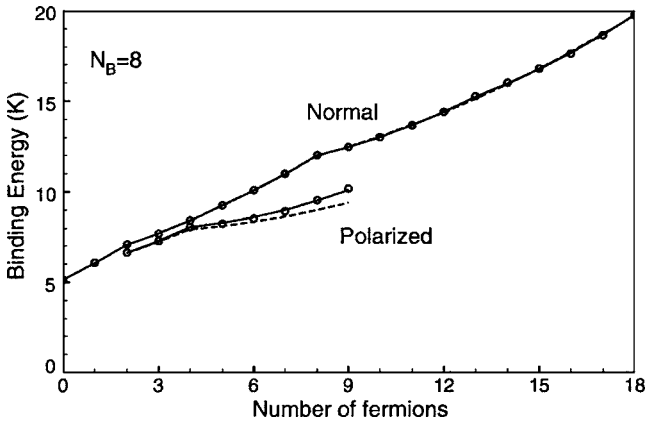

FIG. 7. Comparison of DMC binding energies with the monopole Hamiltonian with spin (continuous line) and without spin terms (dashed line). The circles correspond to the computed DMC values for normal $S_{\max}$ clusters. The lower line corresponds to the fully polarized case, and the upper group to the normal clusters. In both cases $N_B=8$.

The advantage of this operation is that it decouples the determination of the V_{rs} and b_{rs} centroids, so that we can proceed with the former first, as they are the ones that give the global features.

In principle, the six necessary centroids—V_{ss}, V_{sp}, V_{sd}, V_{pp}, V_{pd}, and V_{dd}—could be extracted from Table III. However, this parameter-free choice has large uncertainties and it is better to reserve it as a consistency check with the results of a more precise fit to the energies in Table IV, which we call E_i, $i=0,18$. It is very instructive to start doing the fit by hand, i.e., step by step.

Upon filling, the closed shells become new "cores": $E_2=E_{Cs}$, $E_8=E_{Cp}$,.... The single-particle energies are taken from Table I. Then $E_2=E_{Cs}=E_0+2\varepsilon_s+V_{ss}$. Then V_{ss} is extracted. $E_3=E_{Cs}+\epsilon_p+2V_{sp}\equiv E_{Cs}+\bar{\epsilon}_p$. Then V_{sp} is extracted. To extract V_{pp}, we do not rely on E_4, because it is not purely given in terms of centroids, but on $E_7=E_{Cs}+5\bar{\varepsilon}_p+10V_{pp}$ or $E_8=E_{Cp}=E_{Cs}+6\bar{\varepsilon}_p+15V_{pp}$.

The fit becomes overdetermined, signaling a problem with some basic assumption about the effective interaction, which we shall try to identify later. As of now let us settle for a compromise value of V_{pp}. The next step is $E_9=E_{Cp}+\varepsilon_d+2V_{sd}+6V_{pd}\equiv E_{Cp}+\bar{\varepsilon}_d$ that determines $V_{sd}+3V_{pd}$. As the two matrix elements will only appear in this linear combination, the number of parameters is reduced to five. Finally, for V_{dd} we have the same compromise problem we had for V_{pp}. To find reasonable values for V_{pp} and V_{dd} it was decided to do an overall fit of the five parameters. In principle, the idea does not seem very sound because three parameters are *apparently* well determined. As we shall see, this may not be the case, and the numerical fit will turn out to be sound.

The handmade fit involves $cs\pm1$ states that are common to the $S_{\max}$ and $L_{\max}$ cases in Table IV. In doing the numerical fit, only the $S_{\max}$ states were included. The results for the binding energies in the $N_B=8$ clusters are given in Fig. 7. The agreement is quite excellent, but for the fully polarized case, also shown, there are significant discrepancies that can be cured by introducing the full H_{mS} through a single parameter $b_{rs}=b$ so that the contribution of the second line in Eq. (14) becomes $b[S(S+1)/2-\Sigma_r 3n_r(D_r-n_r)/4(D_r-1)]$. The

Downloaded 29 Jan 2010 to 147.156.182.23. Redistribution subject to AIP license or copyright; see http://jcp.aip.org/jcp/copyright.jsp

TABLE VI. The fitted centroids in K.

	$N_B=8$		$N_B=20$	
	Value	Error	Value	Error
V_{ss}	0.073	0.006	−0.019	0.007
V_{sp}	0.079	0.002	0.080	0.003
V_{pp}	0.081	0.002	0.031	0.003
$(V_{sd}+3V_{pd})/4$	0.078	0.001	0.045	0.001
V_{dd}	0.069	0.001	0.045	0.002
b	0.071	0.005	0.063	0.007

results of the fit are given in Table VI. The fitted and calculated curves become nearly indistinguishable. As noted at the end of Sec. V B, the full energies are rather smooth patterns that tell us little about details. As a first approximation, Fig. 7 for the normal $S_{\max}$ clusters is reasonably well represented by a straight line, which would be the analog of the famous Bethe-Weizsäcker "liquid drop" formula for nuclei. The truly sensitive quantities are the separation energies (chemical potentials) in Eq. (9) and Fig. 4. And, indeed, the true test of the monopole description comes in Fig. 8. A smooth linear approximation to the binding energies would result in a constant. By introducing H_m there is an enormous improvement in that the shell effects at closures are well reproduced (dashed line). However, the more detailed pattern between closures demands the $S(S+1)$ term in the full H_{mS}: the agreement with DMC becomes truly quantitative (full line).

The numerical fit was made for the normal case we have called $S_{\max}$, but Table IV contains another normal mode, $L_{\max}$. As was noted, the handmade fit is the same for both couplings, and it gives results that are almost as good as the numerical fit for $S_{\max}$ and very good ones for $L_{\max}$. But here the numerical fit also does a slightly better job, shown in Fig. 9, where H_{mS} is seen to reproduce beautifully the staggering pattern between $S=0$ and $S=1/2$ states (referred to as the $L_{\max}$ case in Table IV). Here we are faced with some interesting physics: the numerical fit was chosen to find good compromise values for V_{pp} and V_{dd}, but it does slightly better than a fit restricted to those overdetermined parameters. The

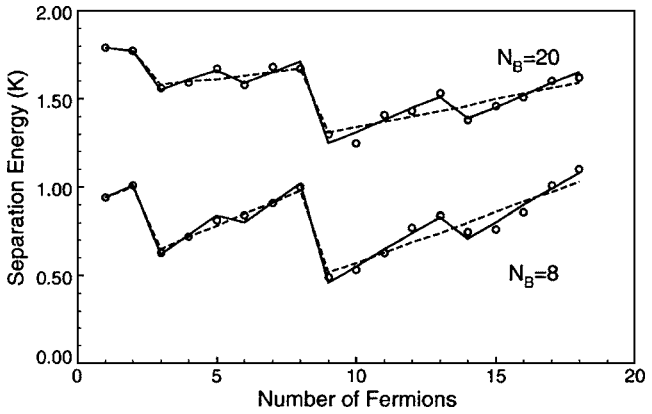

FIG. 8. Comparison of calculated separation energies with the monopole Hamiltonian with spin (H_{mS}, continuous line) and without spin terms (H_m, dashed line) for $S_{\max}$ states. The circles correspond to the computed DMC values. The lower group corresponds to $N_B=8$, and the upper group to $N_B=20$.

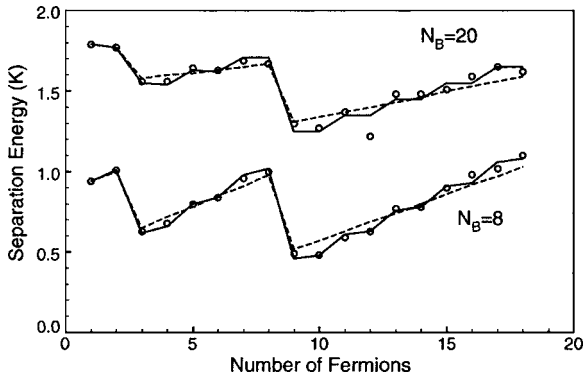

FIG. 9. Same as Fig. 8, but for clusters with $L_{\max}$.

hint is that the other three parameters are not as well determined as the "handmade" fit suggests. The most likely reason is to be found in size effects: as fermions are added, the overall radius evolves, and for a self-bound system it should go asymptotically as $N_F^{1/3}$. [A strong indication in this sense will be found in Fig. 10.] Therefore, the effective matrix elements should also evolve in a way our simplified H_{mS} ignores: The numerical fit then emerges as the sound and natural way to define a best compromise value, not only for V_{pp} and V_{dd} but for all the monopole parameters.

Finally, Table VII compares the centroids V_{rs}^0 and V_{rs}^1 obtained with the fit to the 19 normal $S_{\max}$ clusters with the values obtained directly from the DMC calculation of two-fermion states, again with a very good agreement (within the large errors of about 0.04 K associated with the latter), thus confirming the consistency of the effective interaction interpretation.

It appears that very hard DMC calculations lead to results amenable to a very simple and cogent interpretation in terms of the monopole Hamiltonians H_{mS}. The $S(S+1)$ contribution is particularly interesting: Fig. 7 suggests the idea that for large enough number of fermions the polarized clusters could become ground states. Though this is only a

TABLE VII. The two-fermion centroids as obtained from the effective interaction (columns labeled Eff.) compared with the DMC computed values.

	$S=0$		$S=1$	
	Eff.	DMC	Eff.	DMC
		$N_B=8$		
ss	7.09	7.09		
sp	6.57	6.61	6.64	6.65
pp	6.10	6.14	6.17	6.19
sd	5.94	5.99	6.02	6.01
pd	5.46	5.49	5.54	5.51
dd	4.84	4.86	4.91	4.94
		$N_B=20$		
ss	37.32	37.33		
sp	36.97	37.06	37.04	37.05
pp	36.58	36.73	36.64	36.74
sd	36.44	36.47	36.50	36.49
pd	36.04	36.15	36.10	36.19
dd	35.54	35.54	35.61	35.70

Downloaded 29 Jan 2010 to 147.156.182.23. Redistribution subject to AIP license or copyright; see http://jcp.aip.org/jcp/copyright.jsp

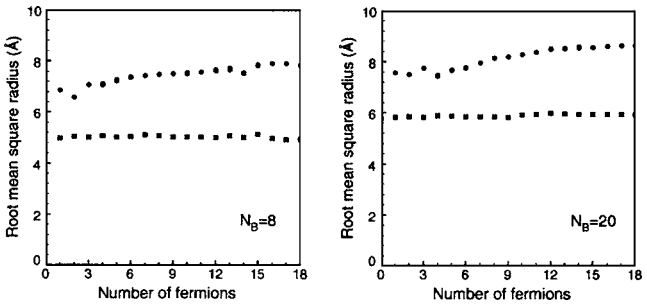

FIG. 10. The values of the root-mean-square radii (in Å) for bosons (squares) and fermions (circles), referred to the center-of-mass of the cluster, as a function of the number of fermions N_F in the cluster. The number of bosons are fixed to N_B=8 and 20.

speculation, it may also be taken as a strong invitation to push the study of mixed clusters much further.

VII. THE SHAPE OF MIXED CLUSTERS

A. Normal mixed clusters

In this section we present several figures related to the shape of mixed clusters. In Fig. 10 there are the values of the root-mean-square radii for bosons and fermions referred to the center of mass of the cluster for the selected cases N_B =8 and 20. There are some fluctuations, probably related to the use of the mixed estimator method to compute these radii, and thus dependent on the quality of the importance sampling wave function. Apart from these fluctuations, the most noticeable properties which emerge from these plots are the almost constant bosonic radii and the smooth growing of the fermionic radii. These manifest clearly the representation of the cluster as a quite rigid bosonic core with a halo of fermions.

This picture is confirmed by the plots of Fig. 11, where the one-body distributions of bosons and fermions with respect to the center of mass of the mixed cluster are displayed. These distributions are given by

$$\rho_M(r) = \langle \Psi | \sum_{i=1}^{N_M} \delta(\mathbf{r} - [\mathbf{r}_i - \mathbf{R}]) | \Psi \rangle,$$

where label M stands for B (bosons) or F (fermions), N_M is the number of atoms of the given species, and R is the center of mass of the full drop. Given that these distributions may have an angular dependence for open shells, we have computed their spherical average. The distributions are normalized to the number of particles of a given species,

$$\int \rho_M(r) d\mathbf{r} = N_M.$$

We observe in Fig. 11 that bosons are located in the same central region, being slightly compressed as the number of fermions increases. This shrinking is more important for the light N_B=8 cluster, and is almost negligible when N_B=20. With respect to the distributions of fermions, they are clearly located at the surface of the bosonic subcluster, with a small penetration near the center of the drop in the case of N_B=8, more important for larger values of the number of fermions. In the case of N_B=20 the dominating picture is that of a rigid core of bosons with a fermionic halo.

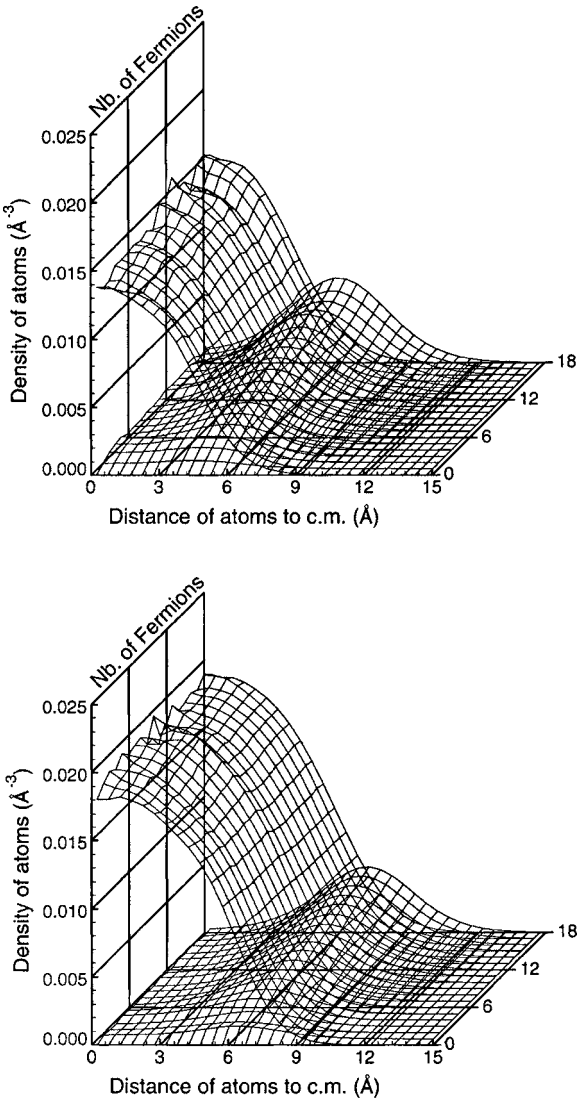

FIG. 11. The density distributions (in Å^{-3}) of bosons and fermions with respect to the center of mass of the cluster for the two selected N_B=8 and 20 cases.

A complementary information about the shape of clusters is provided by the two-body distributions,

$$\rho_M(\mathbf{r}, \mathbf{r}') = \frac{2}{N_M(N_M-1)} \langle \Psi | \sum_{i<j}^{N_M} \delta(\mathbf{r} - \mathbf{r}_i) \delta(\mathbf{r}' - \mathbf{r}_j) | \Psi \rangle,$$

which is normalized to 1.

Because of the finite size of the system under consideration, this distribution function depends on two coordinates, $\mathbf{r}$ and $\mathbf{r}'$, or, equivalently, on the distance of the center of mass of the pair $[(\mathbf{r}+\mathbf{r}')/2]$ to the center of mass of the system and the relative distance $(\mathbf{r}-\mathbf{r}')$ of the two particles, thus producing a function very difficult to plot. In order to get a more friendly quantity, we have averaged the above two-body distribution with respect to its center of mass and for the remaining dependence we have computed the spherical average. The reduced pair distribution so obtained is now normalized to 1,

Downloaded 29 Jan 2010 to 147.156.182.23. Redistribution subject to AIP license or copyright; see http://jcp.aip.org/jcp/copyright.jsp

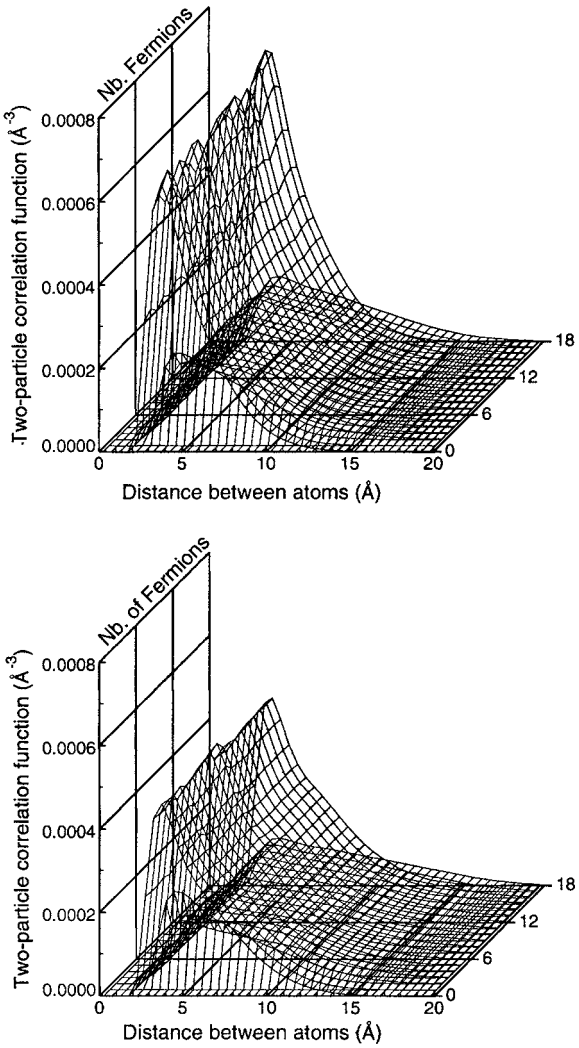

FIG. 12. The boson-boson and fermion-fermion distributions (in Å^{-3}) for the two selected cases, $N_B=8$ and 20.

$$\int \rho_{12}(r)d\mathbf{r} = 1.$$

The boson-boson and fermion-fermion distributions are shown in Fig. 12.

B. Polarized mixed clusters

There are noticeable similarities between the distribution functions related to polarized systems and those corresponding to normal clusters. The subcluster of bosons is again *hard*, its radius being practically independent of the number of spin-aligned fermions N_F. Differences with respect to the unpolarized cluster appear when comparing the root-mean-square radii of fermions, as shown in Fig. 13, where the fermion halo in the polarized clusters is larger than in the unpolarized case.

Something similar happens with the density distributions of bosons or fermions with respect to the center of mass. The former remains basically unaltered when the number of fermions grows, and the latter follows the same pattern as in the case of unpolarized clusters.

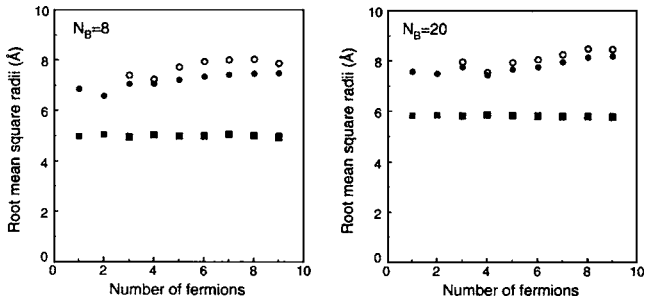

FIG. 13. The values of the root-mean-square radii (in Å) referred to the center of mass for bosons (filled squares) and fermions (filled circles for normal clusters and open circles for polarized clusters) as a function of the number of fermions N_F in the cluster. The number of bosons is fixed to $N_B=8$ (left panel) and 20 (right panel).

There is, however, a remarkable fact in connection with the two-body distributions and, specifically, the fermion-fermion distributions. These distributions are shown in Fig. 14 for the two selected cases $N=8$ and 20. As can be seen there, the fermion-fermion distributions are very different from those obtained for the normal systems: the rise near 4 Å is much less pronounced and the range is much larger, suggesting that the fermions are either less correlated or subjected to a long-range correlation.

In order to appreciate the differences in the density distribution functions for normal and polarized clusters, we have plotted them in Fig. 15 for $N_F=9$ and $N_B=8$. Apart

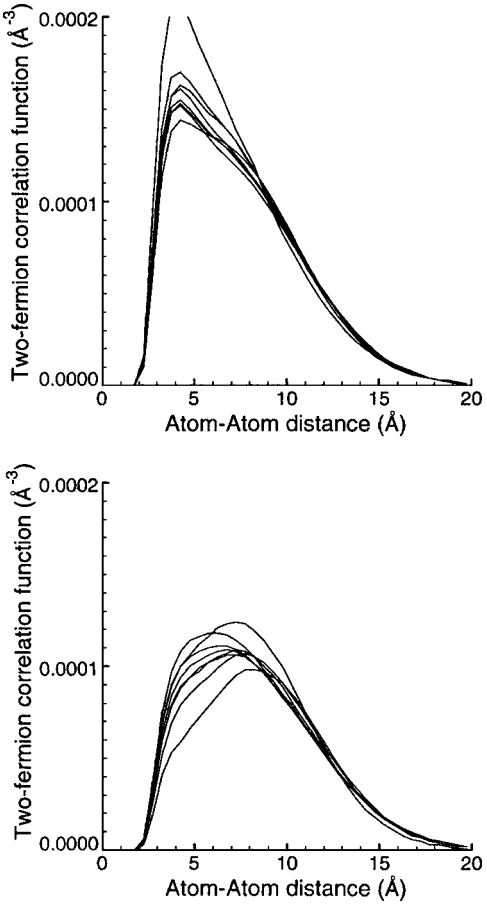

FIG. 14. The fermion-fermion distributions (in Å^{-3}) for $N_B=8$ and unpolarized (top) and fully polarized (bottom) clusters.

Downloaded 29 Jan 2010 to 147.156.182.23. Redistribution subject to AIP license or copyright; see http://jcp.aip.org/jcp/copyright.jsp

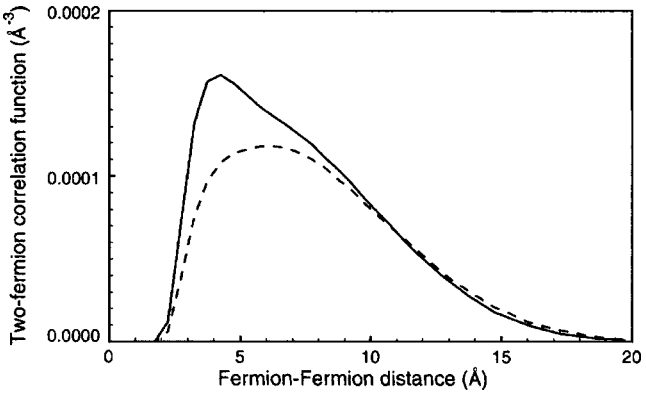

FIG. 15. Comparison of the fermion-fermion distributions for clusters with N_B=8 and N_F=9. The dashed line corresponds to the polarized cluster and the continuous line to the normal cluster.

from a clear change in the shape, the peak of the normal case is close to 4 Å, while for the polarized cluster it is close to 7 Å.

VIII. SUMMARY AND CONCLUSIONS

This work has been devoted to a detailed analysis of clusters made of ^{4}He and ^{3}He atoms. This new analysis was motivated by the improved knowledge of the ordering of single-particle orbitals, obtained after a systematic study of the spectrum of a single ^{3}He atom bound to a core of ^{4}He atoms,[18] which is expected to provide the optimal importance sampling trial function for the DMC calculation. The study has concentrated on clusters having a sufficiently large number of ^{4}He atoms so as to offer a simplified pattern: the bosonic constituents arrange themselves as a quite rigid core, whereas the fermionic atoms are distributed in the surface of the bosonic subcluster, producing a halo. This arrangement, previously obtained by means of density-functional methods, has been confirmed and pushed down to systems with a small number of constituents.

One of the primary aims was to check the previously obtained stability map,[8] after the optimization of the importance sampling function, as well as the improvement of the fermionic nodal surfaces. No significant change occurred, and large instability islands are still predicted for a small ($N_B \leqslant 3$) number of ^{4}He atoms.

The determination of correlation functions, particularly the fermion-fermion distribution functions, as well as the analysis in terms of an effective interaction model suggests that the residual interactions between the fermions is very weak, of the order of the computational precision achieved (near 0.1 K). This fact is also reflected in the insensitivity of the energies to the (L,S) quantum numbers, the spectrum being essentially determined by the configuration.

In addition to the *normal* fermionic phase, with a small value of the spin, we have also analyzed the possibility of having a *ferromagnetic* phase with all spins aligned. The normal phase is energetically favored but the ferromagnetic one gives rise to bound states, even for a moderately large number of ^{3}He atoms. For example, a cluster with 20 bosons is able to bind up to six fermions, but beyond that number the system is above the dissociation limit. Nevertheless, because of the large values of the spin for the ferromagnetic phase, one may expect these unbound states to be long-lived, like in the case of polarized liquid ^{3}He, and thus to be experimentally detectable. Perhaps by circulating bosonic clusters through a cold atmosphere of polarized ^{3}He atoms one could create these spin-aligned states, sticking ^{3}He atoms one-by-one to the bosonic seed.

The mixed systems may have a very rich excitation spectrum, because of the gap between the normal and the polarized phase. For example, for N_B=20 and N_F=6 there is a difference of 1 K between the normal state (configuration $1s^2 1p^4$) and the polarized state (configuration $1s^1 1p^3 1d^2$). The analysis of the intermediate filled configurations, such as $1s^2 1p^3 1d^1$ or $1s^2 1p^2 1d^2$, puts heavy demands on the DMC algorithm but it would be relatively simple in the density-functional method. Though it does not seem possible with the present experimental techniques to measure the spectrum, it is worth remembering that the excitation spectrum plays a relevant role in the production abundances of cluster.[34,35]

Finally one should stress the power of the effective monopole interaction analysis that points to the basic simplicity of the DMC results and invites to take on the challenge of unearthing the deep reasons of such simplicity.

ACKNOWLEDGMENTS

This work has been supported by MCyT/FEDER (Spain), Grant No. FIS2004-00912, GV (Spain), Grant No. GV2003-002 and MIUR (Italy), cofin-2001025498. Part of this study was done while R.G. was visiting professor at Universit Louis Pasteur in Strasbourg. One of us (R.G.) acknowledges financial support of the Secretaría de Estado de Educación y Universidades (Spain), Ref. PR2003-0374, as well as DEMOCRITOS by their hospitality.

[1] K. B. Whaley (editor), Special issue of J. Chem. Phys. **115**, 10065 (2001).
[2] *Advances in Quantum Many-Body Theory*, edited by E. Krotscheck and J. Navarro (World Scientific, Singapore, 2002), Vol. 4.
[3] M. Barranco, J. Navarro, and A. Poves, Phys. Rev. Lett. **78**, 4729 (1997).
[4] R. Guardiola and J. Navarro, Phys. Rev. A **71**, 035201 (2005).
[5] R. Guardiola and J. Navarro, Phys. Rev. Lett. **89**, 193401 (2002).
[6] D. Bressanini and G. Morosi, Phys. Rev. Lett. **90**, 133401 (2003).
[7] D. Bressanini, G. Morosi, L. Bertini, and M. Mella, Few-Body Syst. **31**, 199 (2002).
[8] R. Guardiola and J. Navarro, Phys. Rev. A **68**, 055201 (2003).
[9] W. Schöllkopf and J. P. Toennies, Science **266**, 1345 (1994).
[10] W. Schöllkopf and J. P. Toennies, J. Chem. Phys. **104**, 1155 (1996).
[11] R. E. Grisenti, W. Schöllkopf, J. P. Toennies, G. C. Hegerfeldt, T. Köhler, and M. Stoll, Phys. Rev. Lett. **85**, 2284 (2000).
[12] J. P. Toennies (private communication).
[13] F. Dalfovo, Z. Phys. D: At., Mol. Clusters **14**, 263 (1989).
[14] M. Barranco, M. Pi, S. M. Gatica, E. S. Hernández, and J. Navarro, Phys. Rev. B **56**, 8997 (1997).
[15] A. Belić, F. Dalfovo, S. Fantoni, and S. Stringari, Phys. Rev. B **49**, 15253 (1994).
[16] D. Bressanini, M. Zavaglia, M. Mella, and G. Morosi, J. Chem. Phys. **112**, 717 (2000).
[17] E. Krotscheck and R. Zillich, J. Chem. Phys. **115**, 10161 (2001).
[18] S. Fantoni, R. Guardiola, and J. Navarro, Phys. Rev. A **70**, 023206 (2004).
[19] M. Pi, R. Mayol, and M. Barranco, Phys. Rev. Lett. **82**, 3093 (1999).
[20] J. Navarro, A. Poves, M. Barranco, and M. Pi, Phys. Rev. A **69**, 023202 (2004).
[21] S. Nakaichi, T. K. Lin, Y. Akaishi, and H. Tanaka, J. Chem. Phys. **71**,

Downloaded 29 Jan 2010 to 147.156.182.23. Redistribution subject to AIP license or copyright; see http://jcp.aip.org/jcp/copyright.jsp

4430 (1979).
[22] R. A. Aziz, F. R. McCourt, and C. C. K. Wong, Mol. Phys. **61**, 1487 (1987).
[23] P. J. Reynolds, D. M. Ceperley, B. J. Alder, and W. A. Lester, Jr., J. Chem. Phys. **77**, 5593 (1982).
[24] J. W. Moskowitz, K. E. Schmidt, M. A. Lee, and H. M. Kalos, J. Chem. Phys. **77**, 349 (1982).
[25] R. P. Feynman and M. Cohen, Phys. Rev. **102**, 1189 (1956).
[26] K. E. Schmidt, M. A. Lee, M. H. Kalos, and G. V. Chester, Phys. Rev. Lett. **47**, 807 (1981).
[27] V. R. Pandharipande, S. C. Pieper, and R. B. Wiringa, Phys. Rev. B **34**, 4571 (1986).
[28] E. U. Condon and G. H. Shortley, *The Theory of Atomic Spectra* (Cambridge University Press, Cambridge, 1951), see Table I, p. 208.
[29] F. H. Zong, D. M. Ceperley, S. Moroni, and S. Fantoni, Mol. Phys. **201**, 1705 (2003).
[30] J. B. French, in *Isospin in Nuclear Physics*, edited by D. H. Wilkinson (North Holland, Amsterdam, 1969).
[31] A. Abzouzi, E. Caurier, and A. P. Zuker, Phys. Rev. Lett. **66**, 1134 (1991).
[32] J. Duflo and A. P. Zuker, Phys. Rev. C **59**, R2347 (1999).
[33] E. Caurier, G. Martinez-Pinedo, F. Nowacki, A. Poves, and A. Zuker, Rev. Mod. Phys. **77**, 427 (2005).
[34] L. W. Bruch, W. Schöllkopf, and J. P. Toennies, J. Chem. Phys. **177**, 1544 (2002).
[35] R. Brühl, R. Guardiola, A. Kalinin, O. Kornilov, J. Navarro, T. Savas, and J. P. Toennies, Phys. Rev. Lett. **92**, 185301 (2004).

Downloaded 29 Jan 2010 to 147.156.182.23. Redistribution subject to AIP license or copyright; see http://jcp.aip.org/jcp/copyright.jsp